Design, Construction and Control for an Underwater Vehicle Type Sepiida

Miguel Angel Garcia Rangel, Pedro Castillo Garcia, Eduardo Campos, Rogelio Lozano

Design, Construction and Control for an Underwater Vehicle Type Sepiida

Miguel Angel Garcia Rangel, Pedro Castillo Garcia, M Garcia, P Castillo, Eduardo Campos, Rogelio Lozano

Design, Construction and Control for an Underwater Vehicle Type Sepiida

M. Garcia[†], P. Castillo*[†], E. Campos[§] and R. Lozano[†]

[†]*CINVESTAV - IPN, LAFMIA UMI CNRS 3175 -Ciudad de México, México.*
[‡]*Sorbonne Universités - Heudiasyc UMR 7253, Université de Technologie de Compiegne, France.*
[§]*CONACYT-Universidad del Istmo, Tehuantepec, Oaxaca, México*

(Accepted MONTH DAY, YEAR. First published online: MONTH DAY, YEAR)

SUMMARY
A novel underwater vehicle configuration with an operating principle as the Sepiida animal, is presented and developed in this paper. The mathematical equations describing the movements of the vehicle are obtained using the Newton-Euler approach. An analysis of the dynamic model is done for control purposes. A prototype and its embedded system are developed for validating analytically and experimentally the proposed mathematical representation. A real-time characterization of one mass is done to relate the pitch angle with the radio of displacement of the mass. In addition, first validation of the closed-loop system is done using a linear controller.

KEYWORDS: Underwater vehicle design; mathematical representation; movable mass characterization; prototype; glider configuration; real-time validation.

1. Introduction

During the last decades, the use of underwater robots have had increased mainly in civil applications, national security and oceanographic research in tasks of reconnaissance, inspection and monitoring refs. [1, 2]. For example, in February 2017, the group of Shenyang Institute of Automation, CAS, has performed field tests in Mariana Trech to obtain measurements of the environmental variables of the high seas. The study was done at a depth of approximately 6300 meters ref. [3]. Similarly, in ref. [4] the authors explain the obvious need for the acquisition of oceanic data to study and make predictions of Earth's environmental changes. The exploration of deep waters drives the use of Autonomous Underwater Vehicles (AUVs), because the ability of these vehicles allows to reach environments that are impractical to attain by conventional methods refs.[5–7].

One of the main problems when working with underwater vehicles is to endow them the capacity to stay working long time and produce movements at the same time with low energy consumption. Batteries are currently used as power source nevertheless they need to be recharged each given time especially when the vehicle is emerging or submerging because it uses an important quantity of energy. Vehicle configuration is also important when design an underwater prototype because its form will increase or decrease hydrodynamics phenomena when it is moving refs. [8, 9].

Within the AUVs configurations for this kind of tasks the glider-type vehicles are the most popular because they have a low energy consumption. They can operate with vector propels (hybrid) refs. [10, 11] or by means of displacement of mobile masses and physical properties refs. [12–14]. This kind of vehicles can produce movements modifying

* Corresponding author at: Pedro Castillo. E-mail: castillo@hds.utc.fr

its center of mass to control the pitch and roll angles, to change the buoyancy it moves fluids by means of a ballast tank refs. [12, 15]

Several works related to the design and control of glider-type vehicles can be found in the literature refs. [16,17]. For example; in ref. [18] the authors consider the configuration of the vehicle a bladder that is filled to submerge and empty to emerge, which implies less energy consumption. In ref. [19], the configuration of the vehicle has the property of being modular in order to increase the actuators and act all their degrees of freedom.

In ref. [20] the authors propose to study the effect of buoyancy in the pitch and heave dynamics of an AUV. They propose a technique that specifically compensates this effect and identifies the parameters of the model from the experimental data. In ref. [21], the authors propose a PID fuzzy adaptive controller for compensating uncertainties in the parameters in a nonlinear MIMO system of an AUV. Others works propose the use of controllers based on saturation functions for bounding the control input, for example in ref. [22], the authors propose a nonlinear algorithm with saturation functions and variables parameters to regulate the controller. The stability analysis is based on the Lyapunov theory. The controller is used in an AUV for path tracking.

The Korean for Ocean Research and Development Institute (KORDI) proposes a glider-type vehicle called ISiMI. The main task for this vehicle is to be a test-bed for the development and validation of algorithms when the vehicle is navigating in basins. In this work an analysis of the hull of the prototype is done using the profile proposed by Myring ref. [23], to reduce the drag coefficients. The analysis is made in simulation with experimental tests ref. [24]. In ref. [8] the authors describes the development and validation of a nonlinear simulation model of six degrees of freedom for the REMUS vehicle, taking into account the equations that determine the coefficients, as well as the nonlinear dynamics to obtain a better approximation between the vehicle data collected in experiments carried out at sea. Some underwater vehicles are modular with low cost, they are used mainly in some applications of cartography, inspection, localization, collision avoidance, 3D reconstruction, mapping, and tracking ref. [25]. In ref. [8], the author proposes a nonlinear model, for the REMUS vehicle, taking into account nonlinear coefficients and parameters close to the real vehicle, the goal was to obtain good results when simulating the collected data from experiments carried out at sea.

Our challenge is to propose a configuration for a underwater vehicle with large autonomy and reducing hydrodynamics effects, the configuration adopted for this work is the glider. Based on the literature ref. [18] the best option to stabilize a glider in depth, with low power consumption, is by means of a combination of mobile mass coordinated with a ballast tank to reach a desired depth of operation. In underwater vehicles the ballast tanks are used to allow the vehicle to submerge or emerge changing its buoyancy property.

Our contribution comes from the study and validation of the dynamic model, calculating analytically some of the main moments and hydrodynamic parameters, which are compared with a Computational Fluid Dynamics (CFD) software. The built of a prototype considering the previous analytical study establishes the practical contribution. In addition, a characterization of the mobile mass is made experimentally in open loop. The dynamic model and the prototype are validated using a linear algorithm for controlling the pitch angle.

The outline of the paper is the following: in section 2 general equations and phenomena affecting our vehicle are described, the dynamic model of our Sepiida vehicle configuration is developed in section 3. The prototype build and the embedded system is introduced in section 4, here an analysis of the hydrodynamic parameters is presented. In section 5, experimental results are presented to parametrize the effect of the mobile mass in the pitch angle. Graphs depicting the performance of a linear control algorithm are shown in section 6. Finally discussion about this work and future developments are stated in section 7.

2. Preliminaries - General model

Dynamically an underwater vehicle can be considered as a rigid body of 6 degrees of freedom. For obtaining the dynamic model of this kind of vehicles, we are going to used the general notation for submarine vehicles populated the Society of Naval Architects and Marine Engineers (SNAME) ref. [26]. For this, an inertial frame $I = (X_I, Y_I, Z_I)$ is defined for relating its position $b = (x, y, z)^T$; a body frame $B = (X_B, Y_B, Z_B)$ is proposed with the origin at the center of buoyancy (CB) of the vehicle and its axes aligned with the main axes of the vehicle, see Figure 1. Axis X_B is fixed along the longitudinal axis of the vehicle (positive in the direction of the nose of the submarine), Y_B is defined to the body located in the plane of the wings and finally Z_B is placed in the orthogonal direction to the longitudinal plane.

The forces acting on the vehicle can be represented into the inertial frame by means of a rotation matrix $\mathbf{R}$. This matrix has the following properties; $\mathbf{R}_{3\times3}$, orthogonal $\mathbf{R}^{-1} = \mathbf{R}^T$ and its determinant $\det(\mathbf{R})$=1.

Euler's angles are used to describe the orientation of the vehicle by means of 3 rotations of the rigid body around specific axis of coordinate. These angles are defined as yaw ψ, pitch θ and roll ϕ. For our study we represent in the coordinate system as: ψ positive in clockwise direction, seen from the top, the angle θ is positive when the nose is pointing up, and the angle ϕ is positive with the right wing down, as shown Figure 1.

The position of the vehicle, $\mathbf{b} = (x, y, z)^T$, is the vector of the origin of the inertial frame at the origin of the body frame. The vehicle moves with the translational velocity $\mathbf{v} = (v_a, v_b, v_c)^T$ and rotates with angular velocity $\mathbf{\Omega} = (\Omega_a, \Omega_b, \Omega_c)^T$, both vectors expressed in the coordinate system of the body. The angular velocity $\mathbf{\Omega}$, expressed in terms of Euler angles is defined as:

$$\begin{bmatrix} \dot{\phi} \\ \dot{\theta} \\ \dot{\psi} \end{bmatrix} = \begin{bmatrix} 1 & \tan\theta \sin\phi & \cos\phi \tan\theta \\ 0 & \cos\phi & -\sin\phi \\ 0 & \frac{1}{\cos\theta}\sin\phi & \frac{1}{\cos\theta}\cos\phi \end{bmatrix} \Omega \tag{1}$$

The kinematics of the vehicle can be defined as:

$$\begin{aligned} \dot{\mathbf{R}} &= \mathbf{R}\hat{\mathbf{\Omega}} \\ \dot{\mathbf{b}} &= \mathbf{R}\mathbf{v} \end{aligned} \tag{2}$$

where $(\hat{})$ denotes the skew matrix, proposed in ref. [27] and satisfies $\hat{a}b = a \times b$.

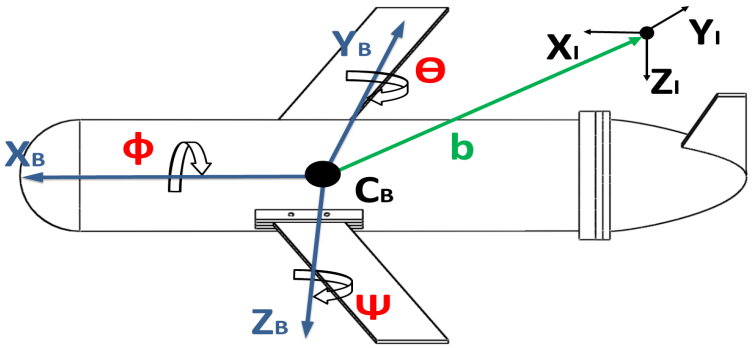

Fig. 1. References frames, vector position and attitude representation in the glider vehicle.

From Newton laws and (2), the following expressions can be deduced

$$\begin{pmatrix} \dot{\mathbf{v}} \\ \dot{\mathbf{\Omega}} \end{pmatrix} = \begin{pmatrix} \mathbf{M}_a^{-1}\bar{\mathbf{F}} \\ \mathbf{J}^{-1}\bar{\mathbf{T}} \end{pmatrix} \tag{3}$$

where $\mathbf{M}_a$ means the inertial matrix and is the sum of body and added mass, $\bar{\mathbf{F}}$ denotes the total forces, $\mathbf{J}$ introduces the tensor of inertia, $\bar{\mathbf{T}}$ represents the total torques.

For a precise mathematical model it should be necessary to consider the physical properties of the prototype such as the hydrodynamic phenomena which depends mainly on the shape of the vehicle ref. [28]. The glider configuration has a cylindrical shape that minimizes hydrodynamics effects with this geometry, this implies that the parameters of the aggregate mass, drag and lift will depend mainly of the position and form of the wings ref. [23]. With this configuration (see Figure 1) and without loss of generality, it is possible to consider that the lateral moment is mechanically stable ($\phi \approx 0$).

When the vehicle is moving, an angle of attack, α, is present producing hydrodynamics effects, theses parameters, H_p, can be defined as

$$H_p = \frac{1}{2}\rho C_\alpha A V^2 \tag{4}$$

where A is the contact surface in the axis of movement of the prototype, ρ represents the density of the fluid, C_α defines a coefficient depending on the parameter α, and V denotes the velocity of the vehicle. Equations (2)-(3) define the general dynamic model of an underwater vehicle.

3. Sepiida dynamic model

The prototype proposed in this work has a torpedo shape without external propellers for moving itself. Some ideas taken from refs. [13, 27] have inspire us for modeling and designing our prototype. Our prototype has a glider form with the Sepiida configuration to move. Therefore, the prototype will be equipped with a bladder for changing the fluid volume and a mobile mass to modify the center of mass, see Figure 2. The mobile mass will produce small separation between the center of gravity CG and the center of buoyancy CB, producing at the same time movement in the pitch angle θ. Therefore, two controls inputs can be deduced for this vehicle, one (u_l) for specifying the rate of change of the ballast mass m_l with a fixed position r_l and the other one (u_m) for controlling the position r_m of the mobile mass.

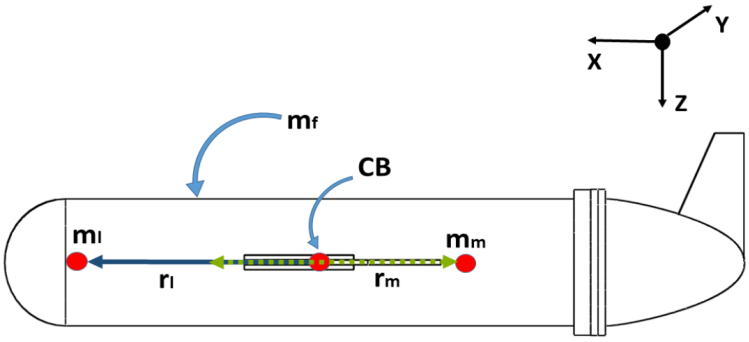

Fig. 2. Masses representation in the vehicle.

The total mass of the vehicle m_v is the sum of the terms: $m_v = m_f + m_l + m_m$, where m_f is the mass of the fixed and uniformly distributed fuselage, m_l corresponds to the total variable mass due to the ballast pumps, for our case it is assumed that the mass of the ballast does not change and only moves from one side to the other of the vehicle. The mobile mass is m_m and aids the movement of pitch.

The total buoyancy, m_{tb} is related mainly with the quantity of the displaced fluid of m_l, defined as $m_{\Delta f}$, such that $m_{tb} = m_v - m_{\Delta f}$ implying that the buoyancy is negative when $m_{tb} > 0$ and positive when $m_{tb} < 0$, as shown in Figure 3.

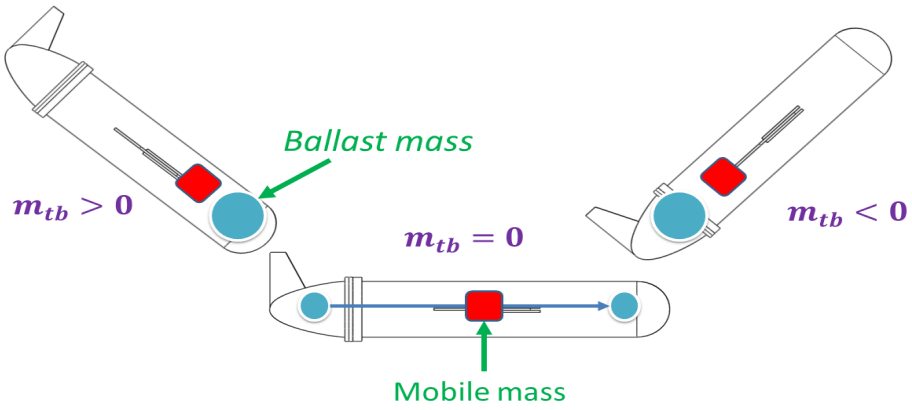

Fig. 3. Total buoyancy acting in the vehicle.

Without loss of generality and from Figure 2, it is possible to consider the vehicle with only a movable mass, $\bar{m}$, moving in the longitudinal and vertical axes with a variable radio $\mathbf{r}_{\bar{m}}$ controlled by $\bar{\mathbf{u}}$ as showing in Figure 4. In addition, we can consider a variable mass, $m_{\Delta f}$, acting in a neighbor of the CB for changing buoyancy in the vehicle. The movable mass is a combination of m_l and m_m.

From Figure 4 notice that when the movable mass is moving, linear momentums are produced. Therefore the following relation can be defined for linear velocities

$$\dot{\mathbf{r}}_{\bar{m}} = \frac{1}{\bar{m}}\mathbf{P} - \mathbf{v} - \mathbf{\Omega} \times \mathbf{r}_{\bar{m}} \tag{5}$$

where $\mathbf{P}$ defines a linear momentum of $\bar{m}$.

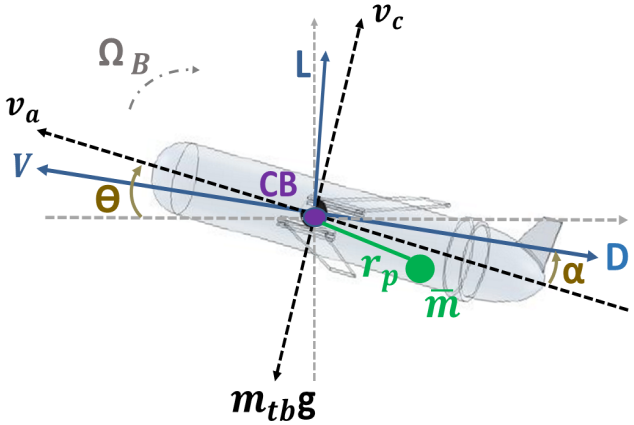

Fig. 4. Forces acting in the underwater vehicle

Observe from (4) that the hydrodynamic parameters are related with the angle of attack and the velocity of the vehicle. Notice that the vehicle has three velocities; two linear (v_a in the x axis and v_c in the z axis), and one rotational in pitch (Ω_b). Therefore the drag (D) and lift (L) forces and the viscous moment (M_{DL}) can be represented by

$$D \approx (K_{D_o} + K_D\alpha^2)(v_a^2 + v_c^2), \tag{6}$$

$$L \approx (K_{L_o} + K_L\alpha)(v_a^2 + v_c^2), \tag{7}$$

$$M_{DL} \approx (K_{M_o} + K_M\alpha)(v_a^2 + v_c^2) + K_{\Omega_b^1}\Omega_b + K_{\Omega_b^2}\Omega_b^2 \tag{8}$$

where the K_i is a constant coefficient, $K_{\Omega_b^1}$ and $K_{\Omega_b^2}$ represent the rotational damping matrices for the linear and quadratic damping terms, respectively, more details see ref. [13].

As previously explained this kind of vehicles has the advantage/ disadvantage to move only in the plane $X_I - Z_I$, thus the main analysis is performed on these axes with a pitch movement. The main variables describing the model in this plane are defined as:

$$\begin{gathered}\mathbf{b} = \begin{pmatrix} x \\ 0 \\ z \end{pmatrix}; \quad \mathbf{R} = \begin{pmatrix} \cos\theta & 0 & \sin\theta \\ 0 & 1 & 0 \\ -\sin\theta & 0 & \cos\theta \end{pmatrix}; \quad \mathbf{v} = \begin{pmatrix} v_a \\ 0 \\ v_c \end{pmatrix}; \quad \mathbf{\Omega} = \begin{pmatrix} 0 \\ \Omega_b \\ 0 \end{pmatrix}; \\ \mathbf{r}_{\bar{m}} = \begin{pmatrix} r_a \\ 0 \\ r_c \end{pmatrix}; \quad \mathbf{P} = \begin{pmatrix} P_a \\ 0 \\ P_c \end{pmatrix}; \quad \bar{\mathbf{u}} = \begin{pmatrix} u_a \\ 0 \\ u_c \end{pmatrix};\end{gathered} \tag{9}$$

Developing equation (1) and (2), it follows that

$$\dot{x} = v_a\cos\theta + v_c\sin\theta \tag{10}$$

$$\dot{z} = -v_a\sin\theta + v_c\cos\theta \tag{11}$$

$$\dot{\theta} = \Omega_b \tag{12}$$

3.1. Forces acting in the longitudinal axis

The main forces acting in this axis are:

- u_a that is the control input to change the radio of the movable mass in the x-axis.
- L and D hydrodynamics forces components.
- $m_{tb}g\sin\theta$ which represents the gravity force due to the displaced fluid and the mass of vehicle.
- Two external forces due to the rate pitch angle Ω_b with respect to the vertical velocity v_c and the other with respect to the linear momentum in the vertical axis P_c.

Therefore this dynamics can be expressed as

$$m_a\dot{v}_a = -u_a + L\sin\alpha - D\cos\alpha - m_{tb}g\sin\theta - (m_cv_c + P_c)\Omega_b$$

where m_a and m_c are the total masses acting on the vehicle in the x and z-axes, respectively, these masses include the added mass in its corresponding axis of movement.

3.2. Forces acting in the vertical axis

For the z axis, the forces are:

- u_c that means the control input for changing the radio of the movable mass in the vertical axis.

- L and D hydrodynamics forces components.
- The gravity force due to the displaced fluid and the mass of vehicle ($m_{tb}g\sin\theta$)
- Two external forces due to the rate pitch angle Ω_b with respect to its longitudinal velocity v_a and the other with respect to the linear momentum in the x-axis P_a.

Therefore the dynamics for the vertical axis can be expressed as:

$$m_c\dot{v}_c = -u_c - L\cos\alpha - D\sin\alpha + m_{tb}g\sin\theta + (m_a v_a + P_a)\Omega_b$$

3.3. Torques acting in the vehicle

By configuration, only the pitch dynamics is presented and studied in this vehicle, then from (3) $J_\theta\dot{\Omega}_b = \tau$, thus from Figure 4, it is easy to analyze that

- The control inputs for moving the movable mass in the vertical and longitudinal axis, produce torques with respect to its opposites variable radios, i.e., $r_c u_a$ and $r_a u_c$.
- The viscous moment, M_{DL} is presented due to the hydrodynamics effects.
- The gravity force exerted by the movable mass produces two torques in the vehicle $\bar{m}gr_a\cos\theta$ and $\bar{m}gr_c\sin\theta$, see Figure 4.
- The angular rate Ω_b will generate two torques related with the linear momentum, in the longitudinal and vertical axes respectively.
- The linear velocities v_a and v_c produce also torques in the vehicle.

From definition we have that the linear momentum is equal to the product of the mass and velocity of an object, i.e., $p = mv$, deriving, it follows that $\dot{p} = m\dot{v} = f$, defining also a force f. Similarly $\dot{v} = a = vw$ where a is the acceleration of the object and w is the angular rate. Therefore a force is related also by its linear momentum and the angular rate, $f = pw$, hence from Figure 4, it easy to deduce that $\tau_{P_a} = P_a\Omega_b r_a$ and $\tau_{P_c} = P_c\Omega_b r_c$.

Remember that the velocities in the x and z axes with respect to the angular rate produce a force in the longitudinal and vertical axes, i.e., $m_c v_c\Omega_b$ and $m_a v_a\Omega_b$, respectively. From definition $w = v/l$ where defines a circular motion at radius l. From our analysis, Ω_b is related with v_a and v_c, if x or z axis are analyzed, respectively. Note also that the torque is defined by the force and distance where this force is applied, in these cases this distance is equal to the radius l. Therefore, it is clear to obtain $m_c v_c v_a$ and $m_a v_a v_c$ for the x and z axes respectively.

Hence the dynamics for the angular moment can be expressed as:

$$J_\theta\dot{\Omega}_b = -r_c u_a + r_a u_c + M_{DL} - \bar{m}g(r_a\cos\theta + r_c\sin\theta) - \Omega_b(r_a P_a + r_c P_c) + (m_c - m_a)v_a v_c$$

3.4. Full dynamics of the Sepiida vehicle

Grouping the dynamics of the underwater vehicle, it follows that

$$\begin{aligned}
m_a\dot{v}_a &= -u_a + L\sin\alpha - D\cos\alpha - m_{tb}g\sin\theta - (m_c v_c + P_c)\Omega_b \\
m_c\dot{v}_c &= -u_c - L\cos\alpha - D\sin\alpha + m_{tb}g\sin\theta + (m_a v_a + P_a)\Omega_b \\
J_\theta\dot{\Omega}_b &= -r_c u_a + r_a u_c + M_{DL} - \bar{m}g(r_a\cos\theta + r_c\sin\theta) - \Omega_b(r_a P_a + r_c P_c) + (m_c - m_a)v_a v_c
\end{aligned}$$

From (5) and Figure 4, it is easy to derive the following

$$\dot{r}_a = \frac{1}{\bar{m}}P_a - v_a - r_c\Omega_b \tag{13}$$

$$\dot{r}_c = \frac{1}{\bar{m}}P_c - v_c - r_a\Omega_b \tag{14}$$

Finally, also from Figure 2 and from definition of linear momentum, it is easy to deduce that

$$\dot{P}_a = u_a \tag{15}$$

$$\dot{P}_c = u_c \tag{16}$$

$$\dot{m}_{\Delta f} = u_l \tag{17}$$

where u_i, $i : a, c$, represents the control input for changing the radio $\mathbf{r}_{\bar{m}}$ of the movable mass $\bar{m}$ in the longitudinal and vertical axes. These control inputs are a fixed combination from u_l and u_m for obtaining specific and desired pitch movements.

3.5. Model analysis

The previous equations (10)-(17) define the kinematics and dynamics of our Sepiida configuration vehicle. An analysis of these equations are developed in the following with the goal to propose a control law to stabilize the vehicle.

3.5.1. Longitudinal dynamics.

Using (12) and (14) into (13) it follows that

$$m_a\dot{v}_a = -\dot{\theta}(v_c(m_c + \bar{m}) + \bar{m}\dot{r}_c) - \dot{\theta}^2\bar{m}r_a - m_{tb}g\sin\theta + L\sin\alpha - D\cos\alpha - u_a \tag{18}$$

when the vehicle is moving a low speed several phenomena appears, for example; the angle of attack could be considered so small, i.e., $\alpha << 1$, hence $\sin\alpha \approx \alpha$ and $\cos\alpha \approx 1$. Similarly, the hydrodynamics parameters depend from the α parameter and the velocity of the vehicle, and therefore they vanish when are smaller, see (6)-(8). Therefore, the following yield

$$L\sin\alpha \approx L\alpha \approx \delta_{\alpha_L}, \tag{19}$$

and

$$-D\cos\alpha \approx -D(v^2) \ll \delta_D, \tag{20}$$

where $\delta_{\alpha_L} << 1$ is a small parameter depending of α and δ_D defines also a parameter depending mainly of the velocity of the vehicle, v, when the attack angle is small, see (6). Rewriting (18), it follows that

$$m_a\dot{v}_a = -\dot{\theta}(v_c(m_c + \bar{m}) + \bar{m}\dot{r}_c) - \dot{\theta}^2\bar{m}r_a - m_{tb}g\sin\theta + \delta_{\alpha_L} + \delta_D - u_a \tag{21}$$

3.5.2. Vertical dynamics.

Similarly, using (13) and (14) into (13), it yields

$$m_c\dot{v}_c = \dot{\theta}(v_a(m_a + \bar{m}) + \bar{m}\dot{r}_a) + \dot{\theta}^2\bar{m}r_a + m_{tb}g\cos\theta - L\cos\alpha - D\sin\alpha - u_c \tag{22}$$

Following a similar analysis used for the longitudinal dynamics, it follows that

$$L\cos\alpha \approx L(v^2) \ll \delta_L \tag{23}$$

and

$$-D\sin\alpha \approx -D\alpha \approx \delta_{\alpha_D} \tag{24}$$

where $\delta_{\alpha_D} << 1$ is a small parameter depending of α and δ_L defines also a parameter depending mainly of the velocity of the vehicle, v, when the attack angle is small, see

(7). Rewriting (22)

$$m_c\dot{v}_c = \dot{\theta}(v_a(m_a+\bar{m})+\bar{m}\dot{r}_a)+\dot{\theta}^2\bar{m}r_a+m_{tb}g\cos\theta+\delta_L+\delta_{\alpha_D}-u_c, \tag{25}$$

3.5.3. Pitch dynamics.

Rewriting (13) using (8) and (14)

$$\begin{aligned} J_\theta\ddot{\theta} = &-r_cu_a+r_au_c+M_{DL}-\bar{m}g(r_a\cos\theta+r_c\sin\theta)-\bar{m}\dot{\theta}r_a(\dot{r}_a+v_a)-\bar{m}\dot{\theta}r_c(\dot{r}_c+v_c)\\ &-2\bar{m}\dot{\theta}^2r_ar_c+(m_c-m_a)v_av_c \end{aligned} \tag{26}$$

Observe from (8) that the viscous moment is related with the angle of attack, the vehicle velocity and the vehicle rate in the pitch angle. Slow velocities mean slow rates in the vehicle producing small viscous moment. Therefore without lost of generality, it is possible to write

$$M_{DL} \approx \delta_{M_{DL}} \tag{27}$$

where $\delta_{M_{DL}}$ is a small parameter. Rewriting the pitch dynamics,

$$\begin{aligned} J_\theta\ddot{\theta} = &-r_cu_a+r_au_c+\delta_{M_{DL}}-\bar{m}g(r_a\cos\theta+r_c\sin\theta)-\bar{m}\dot{\theta}r_a(\dot{r}_a+v_a)-\bar{m}\dot{\theta}r_c(\dot{r}_c+v_c)\\ &-2\bar{m}\dot{\theta}^2r_ar_c+(m_c-m_a)v_av_c \end{aligned} \tag{28}$$

4. Prototype

A prototype is built with the goal to corroborate the dynamics of the vehicle in open loop by applying several conditions for mass characterization.

Our prototype has a cylindrical shape (torpedo configuration), with ailerons, equipped with a bladder for volume change and a mobile mass to modify the center of mass. This configuration allows to minimize the forces of aggregate mass, drag and lift. The fuselage of the prototype is made of aluminum, the main diameter of the hull is 6 inches, with 90 centimeters long with a total weight of 10.85kg, see Figure 5. The embedded system is homemade and contains electronic components and actuators.

In our prototype the ballast is formed by a gasoline pump coupled to a container with the fluid to be moved and at the other end a bladder with a capacity of 1000cm^3 as seen in Figure 6.

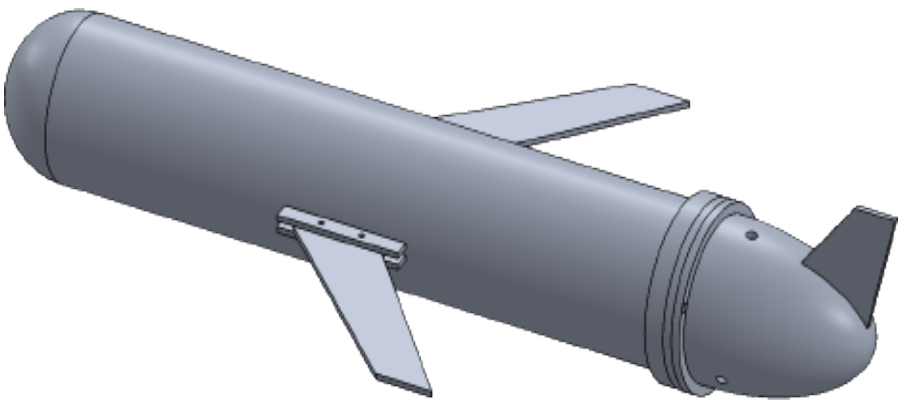

Fig. 5. The Sepiida prototype developped at LAFMIA UMI 3175.

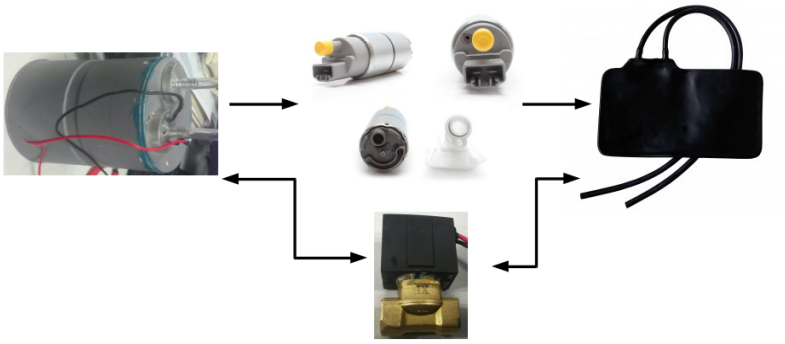

Fig. 6. The ballast containing the fluid to change the buoyancy force.

The embedded system in our Sepiida prototype is responsible for the processing of signals, sensors and actuators. It is composed of a relatively simple architecture containing a Raspberry pi2 card for implementing and computing the algorithms and acquires the environment signals given by the sensors as illustrated in Figure 7.

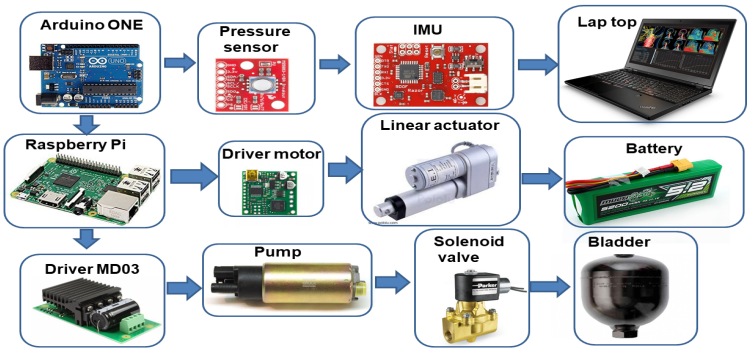

Fig. 7. Embedded system for our prototype Sepiida.

The mobile mass is a system composed of batteries mounted on a linear actuator. This actuator modifies the location of the center of mass when moving a load of 2.09 kg on the x-axis along 4 in. The first characterization was made out-side the vehicle by means of a test-bench that has a load at one end which is balanced with a pistol when it has half the stroke, see Figure 8. The test-bench can be programmed with a routine such that the actuators perform the entire race and it can be possible to tune it with respect an angle of inclination of the test-bench.

Fig. 8. Mobile mass test bench. It is used for finding a first relation between the radio of the actuator, the mobile mass and the angle of inclination of the test bench.

The communication between the Raspberry Pi2 (embedded system) and the ground station is achieved through Secure SHell (SSH), either wired or wireless communication, see Figure 9. Once the communication is established, it is possible to analyze the states of the vehicle, the sensors and the actuators. In addition, with the ground station it is possible to tune or change the algorithms, as well as loading or downloading data from/for new missions.

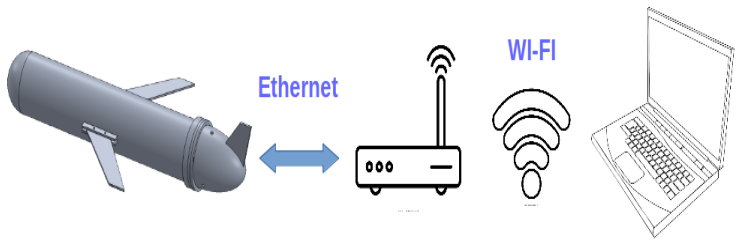

Fig. 9. Glider communication scheme.

4.1. Depth analysis of the prototype

When a vehicle is immersed in a fluid, it is exposed to a pressure that depends on the depth in which it is. A pressure analysis is performed in the prototype, on the hollow parts, to obtain its safety factor. For this analysis the pressure equation of the water column is used $P_r = \rho g h_p$ where P_r is the pressure of the water column on the vehicle, $\rho = 1000\frac{kg}{m^3}$ defines the density of water, h_p represents the depth at which the vehicle is submerged and $g = 9.81\frac{m}{seg^2}$ means the constant of the acceleration of gravity. Considering $h_p = 100$m, the safety factor obtained in the body is 9.56 while in the tail of 8.16, see Figure 10. From the literature for underwater vehicles, it is suggested a safety factor greater than 1, therefore our prototype is capable to support a pressure of 100m.

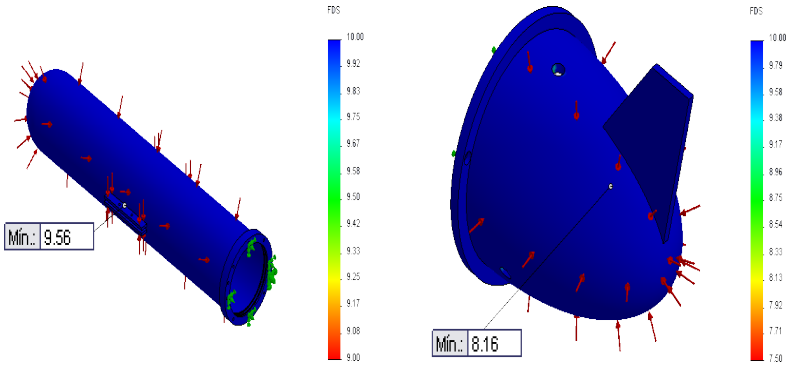

Fig. 10. Depth analysis for the prototype with a depth of 100m.

4.2. Identification of hydrodynamic parameters

Some hydrodynamic parameters are obtained analytically based on Myring helmet profile equations refs. [23, 29] that could describe the contour of the body shown in Figure 11. In this analysis, it is assumed that the origin of the helmet is in the nose of the vehicle, notice that the prototype body is a cylinder with two different spokes due to the flange that joins with the tail of the prototype, where the reservoir of the bladder is located.

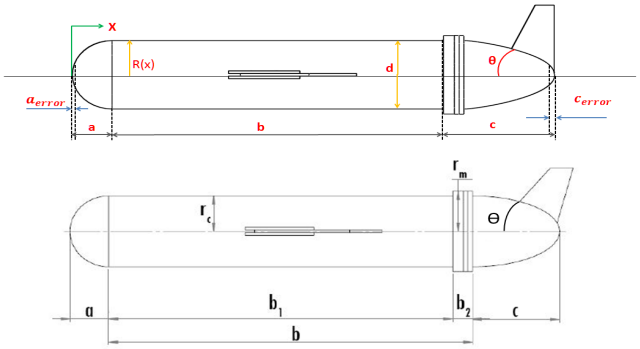

Fig. 11. Sepiida form in our prototype.

The Myring equations in ref. [23] generate an approximate geometry that our prototype has. Observe that using parameters described in Table I a similar form as in our prototype is obtained, see Figures 11 and 12.

Table I . Values for the Myring equations.

Parameters	Value Glider	Units
a	84.14	mm
b	793	mm
b_1	750	mm
b_2	43	mm
c	190	mm
d	168.28	mm
a_{offset}	0	mm
c_{offset}	0	mm
r_c	84.14	mm
r_m	90.25	mm

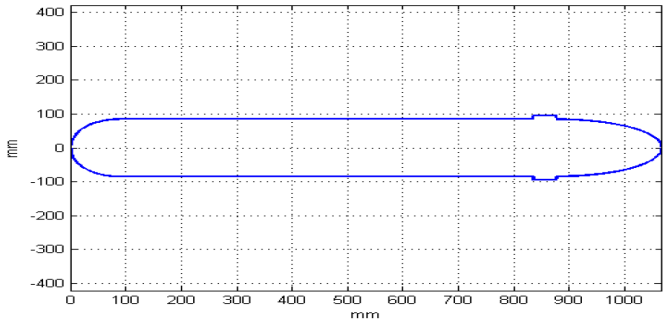

Fig. 12. Form obtained from Myring equations. This form is similar to that in our prototype, see Figure 11.

4.3. Hydrodynamic parameters

Estimate the hydrodynamic parameters is a hard task and sometimes so difficult to obtain. They depend in general of the shape of the prototype and its velocity ref. [30]. Blevins ref. [31] has proposed an empirically method for computing the axial aggregate mass of an ellipsoid, from Figure 13 observe that our prototype could be considered having this form with the semi-major axis having the half of the length of the vehicle and the minor axis the half of the maximum diameter of the vehicle ref. [32].

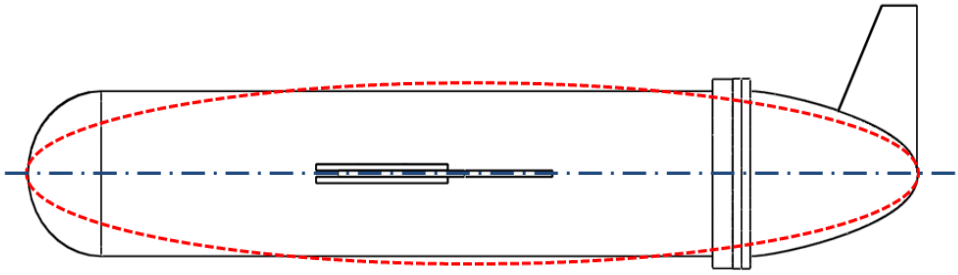

Fig. 13. The Sepiida prototype has an ellipsoid form that is used to estimate its hydrodynamic parameters.

The added transverse mass of the prototype is computed using the *Strip Theory* ref. [8]. It consists in dividing the submerged part of the vehicle into a series of sections, allowing to calculate the hydrodynamic coefficients in two dimensions for the aggregate mass of each section, and then they will be integrated along the length of the body to obtain them in three dimensions.

For obtaining the added mass, we also consider the area of the wings and the Blevins formula for the aggregate mass refs. [31, 32]. The values obtained for our prototype are presented in Table II.

Table II . The hydrodynamic coefficients.

Parameter	Glider	Units
K_{D0}	4.4214	kg/m
K_D	-3.7514	$kg/m/rad^2$
K_β	-50.7908	$kg/m/rad$
K_{L0}	-0.3123	kg/m
K_α	107.891	$kg/m/rad$
K_{MR}	-3.1835	kg/rad
K_P	-48.621	kgs/rad
K_{M0}	0.1859	kg
K_M	-42.4821	kg/rad
K_q	-108.02	kgs/rad
K_{MY}	136.3237	kg/rad
K_r	-21.663	$kg.s/rad$

4.4. Hydrodynamic parameters and added mass using CFD

To obtain the values of the coefficients of hydrodynamic forces and moments, several fluid simulations were carried out with the module *CFD* called *Flow Simulation*. The simulations consist of placing the Computer Aided Design (CAD) of the prototype and fixe it inside a box simulating that it is immersed in the fluid, see Figure 14. Then different values for the angles of attack α and lateral slip β are used for this analysis ref. [33]. To obtain a better result of the values, an approximation is made by least squares.

The results obtained from the added mass by the analytical method are compared with those provided by the CFD software and are shown in Table III. Based on literature and the results obtained, a vehicle with a spherical nose reduces friction which generates greater displacements with the help of the wings, which also increases the lift and stability in the vehicle.

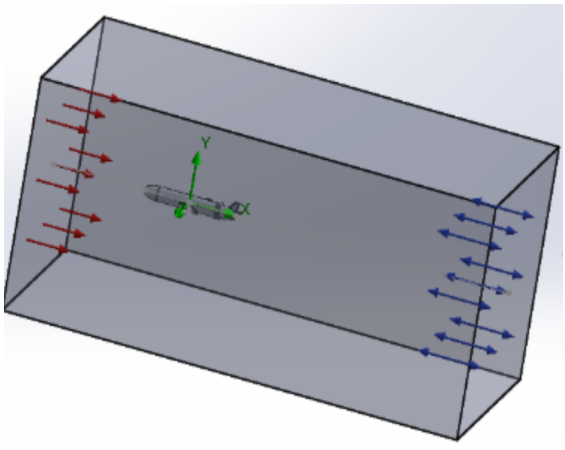

Fig. 14. Simulation to obtain the hydrodynamic coefficients and moment

Table III . The added mass.

Parameter	Glider		
	CFD estimate	Myring	Units
$X_{\dot{u}}$	-0.7739	-	kg
$Y_{\dot{v}}$	-58.9255	-57.2693	kg
$Z_{\dot{w}}$	-22.034	-20.3778	kg
$K_{\dot{p}}$	-0.8065	-	$kg \cdot m^2/rad$
$M_{\dot{q}}$	-15.5673	-14.2225	$kg \cdot m^2/rad$
$N_{\dot{r}}$	-7.7887	-6.4439	$kg \cdot m^2/rad$

5. Simulation and real-time validation

As explained in section 3, Figure 3, two masses are used for producing lateral and vertical displacements in the vehicle. They are the fluid contained in the ballast tank and the other one the mobile mass, both combination are mixed and used to consider a movable mass controlled by u_1 and u_3, see Figure 4.

In this work, firstly we will focus our study for obtaining a relation of the displacement of the mobile mass with respect to the pitch angle.

5.1. Characterization of the mobile mass

To produce the displacement in the mobile mass an input signal, emulating a signal of Pulse-Width Modulation -PWM, is introduced to change its distance r_m in centimeters. After mathematical and physical model analysis, the following relation is obtained to produce the displacement of the mobile mass during the experiments

$$r_m = \frac{PWM * 10.16}{22} \tag{29}$$

where r_m is the distance in centimeters with $0 \leq r_m \leq 10.16$ cm, PWM is the reference signal, such that $0 \leq PWM \leq 22$. These bounds are estimated from the physical properties of the prototype and actuators.

In this first scenario, the idea was to know with good precision the variation between each step of the linear actuator with respect to the pitch angle θ. The tests consisted in modifying the input signal (PWM signal in the experimental part) from 5 to 17 increasing or decreasing one step each 20 sec.

5.1.1. Simulation.

Figure 15 introduces the pitch angle response when increasing the input signal one step each 20 sec. Notice that the maximum values in this graph are ±50°.

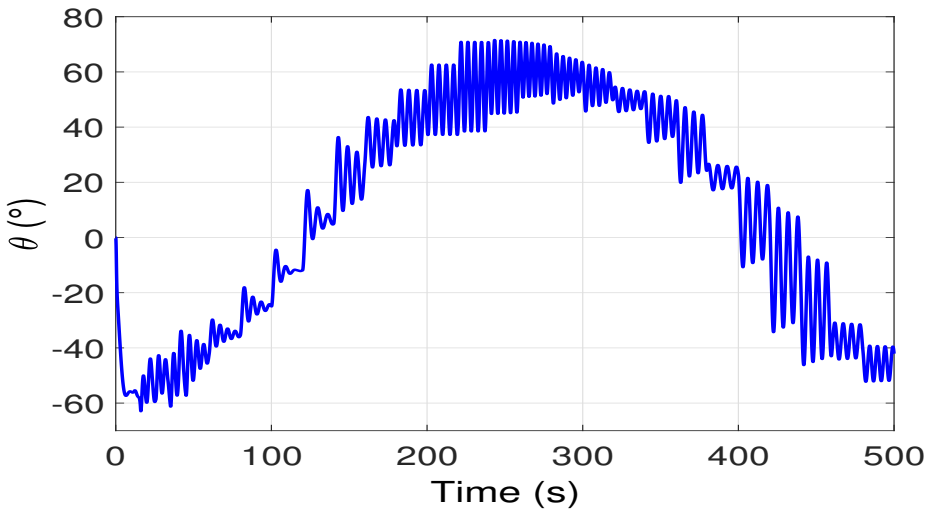

Fig. 15. Pitch angle behavior in simulation when the signal r_m varies every 20 seconds in a range equivalent to the PWM signal of 5 to 17.

5.1.2. Experimental validation.

Same scenario is reproduced in real time using the proposed prototype. The idea was to compare the variation between each step of the linear actuator with respect to the pitch angle θ in simulations and experiments. The test consisted in modifying the PWM signal from 5 to 17 increasing/decreasing one step each 20 sec.

In Figure 16 the relation between the displacement of the mobile mass with respect to the PWM signal applied is illustrated. Notice here that the maximum distance reached is close to 8cm. In Figure 17, the pitch angle behavior is represented graphically to illustrate that the maximum angle that can be reached is ±45° thus, the previous results indicate that we are capable to produce all the pitch angles necessaries for displacing the vehicle.

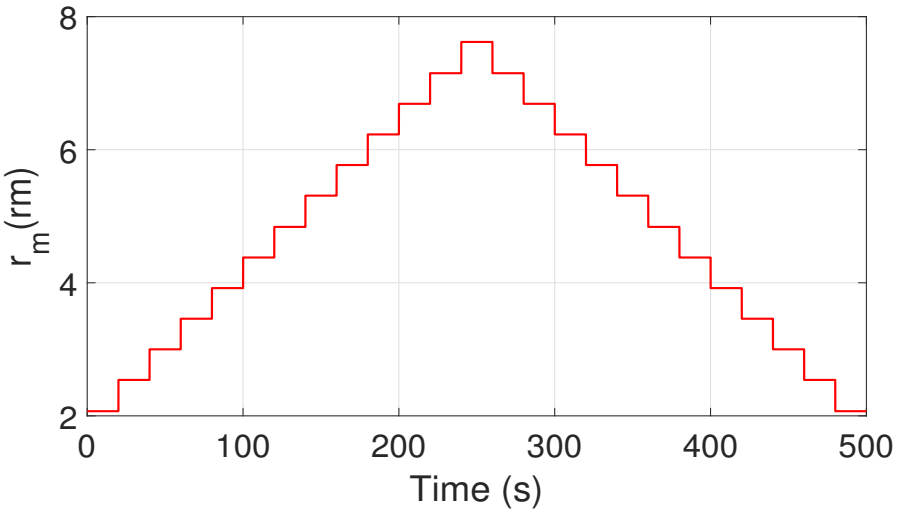

Fig. 16. r_m performance when applying a PWM signal to the mobile mass every 20 seconds.

Notice also from Figures 15 and 16 the similar performance of the pitch angle in simulations and in real-time experiments. This indicate the well parametrization of the proposed dynamic model.

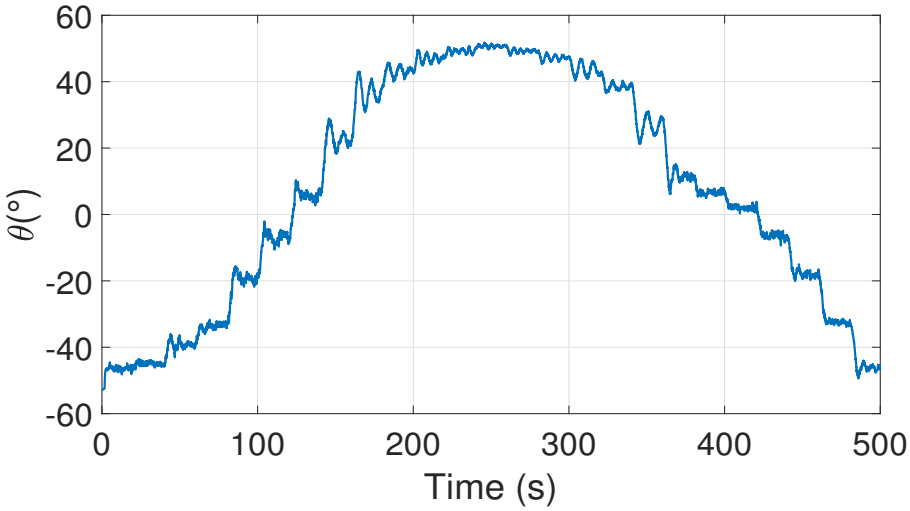

Fig. 17. Pitch response for the first experiment when the PWM is varied from 5 to 17 each time

5.2. Mobile mass performance with abrupt changes in r_m

A a five-step routine is proposed simulating the displacement of the r_m, the goal here is to better analyze the behavior of the theta angle when the mobile mass is changed abruptly. The simulation is done for the following values r_m : 0, 5.08, 10.16, 5.08, 0 in cm.

5.2.1. Simulation result.

In Figure 18 the simulation performance is illustrated, notice here that some oscillations are present in the θ behavior, we consider that these are due to the approximation of the hydrodynamics parameters. Remember that these parameters depend highly in the translational velocity of the vehicle.

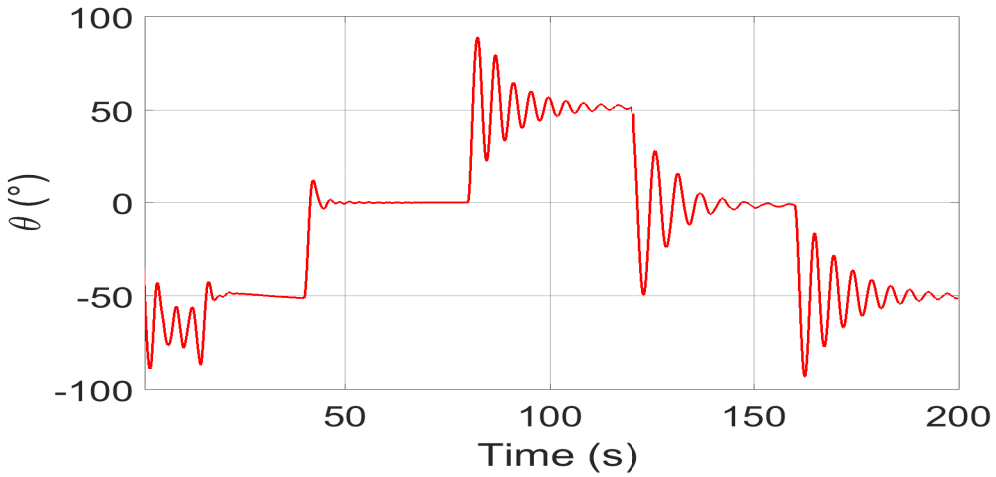

Fig. 18. Pitch behavior when simulating the routine for moving the mobile mass with different values of r_m.

5.2.2. Real-time experiment.

For better tuning the obtained relation PWM *vs* r_m and to analyze the effect generated by the movement of the mobile mass in the prototype, the same routine used in simulation is applied in real time. For reproducing same routine the mobile mass was changing every 40 sec starting from the nose of the vehicle upwards as if it was emerging, that is, $r_m = 0$ cm. Then, it was necessary to wait until the prototype was in the equilibrium position, that is, horizontally with an execution of $r_m = 5.08$ cm, and then place it with the nose downwards as if it was submerging with a displacement of $r_m = 10.16$ cm. Note that in the last case, θ is positive as previously predefined. Figure 19 represents the r_m performance.

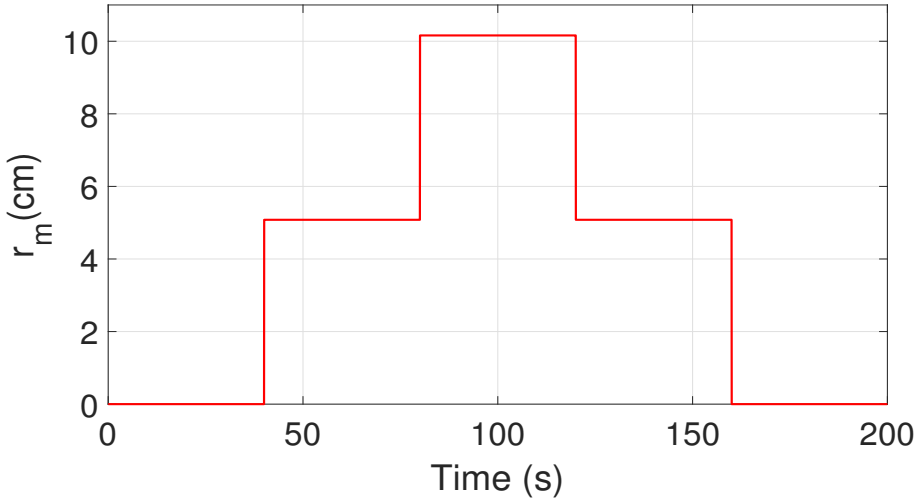

Fig. 19. r_m response when changing the PWM control input every 40 seconds.

The behavior in the pitch angle when applying this routine is shown in Figure 20. Remark that it is only a relation between the PWM applied, the variable radio and the pitch angle. Observe from this figure the oscillations are less than in simulations. This it can be explained by the damping exerted by the water into the vehicle, i.e, the velocity in real time is less than in simulations.

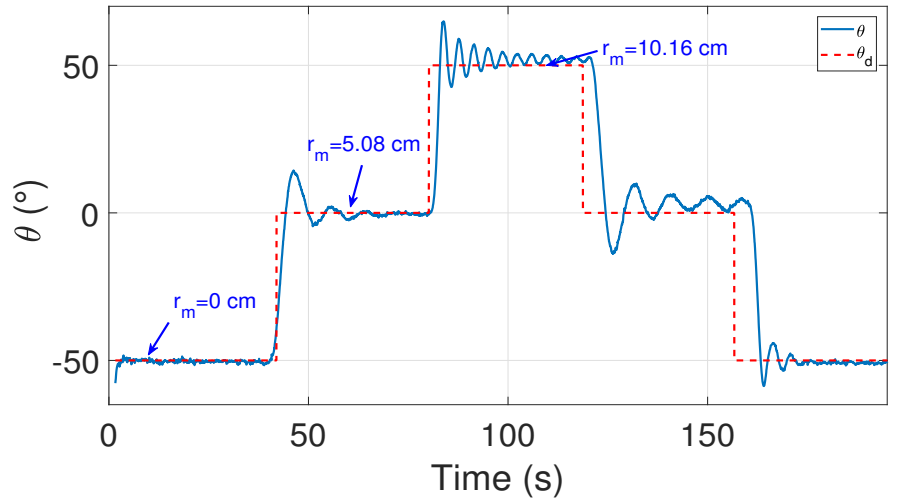

Fig. 20. Pitch angle response for three desired positions. No control is used in this experiment.

5.3. Mobile mass performance with high frequency of PWM

The last experiment consisted in applying several times a constant cycle of the PWM signal to the actuator changing the variable radio of the mobile mass in high frequency, this change in the radio produces changes in the pitch angle as can be observed in Figure 21. The goal here was to analyze the quick response in the pitch movement of the vehicle.

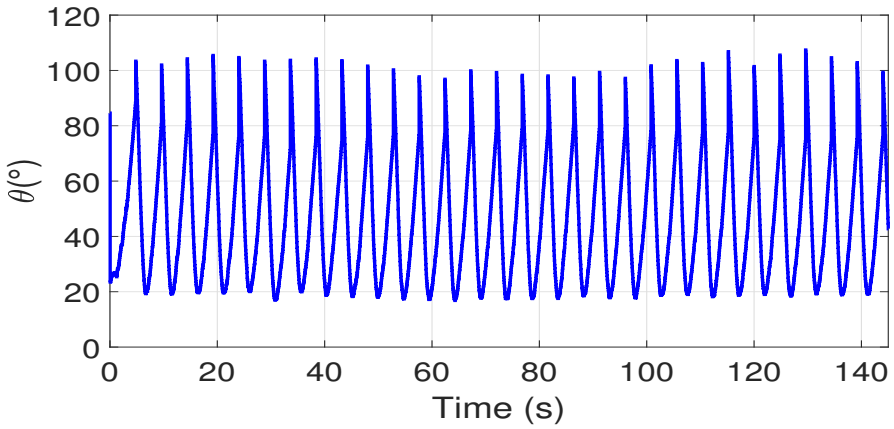

Fig. 21. Pitch angle performance when applying a constant cycle of PWM in the linear actuator for displacing the mobile mass.

6. Control results

Once analyzed the performance of the mobile mass and observed that it is capable to produce torques for controlling the pitch dynamics, the next step is to propose a simple controller for validating the previous results. A PID algorithm is implemented in the embedded system of the prototype for tracking a desired reference, in this case we have chosen a $\sin(\cdot)$ function. Gains control parameters were tuned manually to obtain an acceptable performance from the practical point of view. The experimental results can be analyzed in Figure 22, notice here that the desired amplitude for the $\sin(\cdot)$ function is $\pm 30°$.

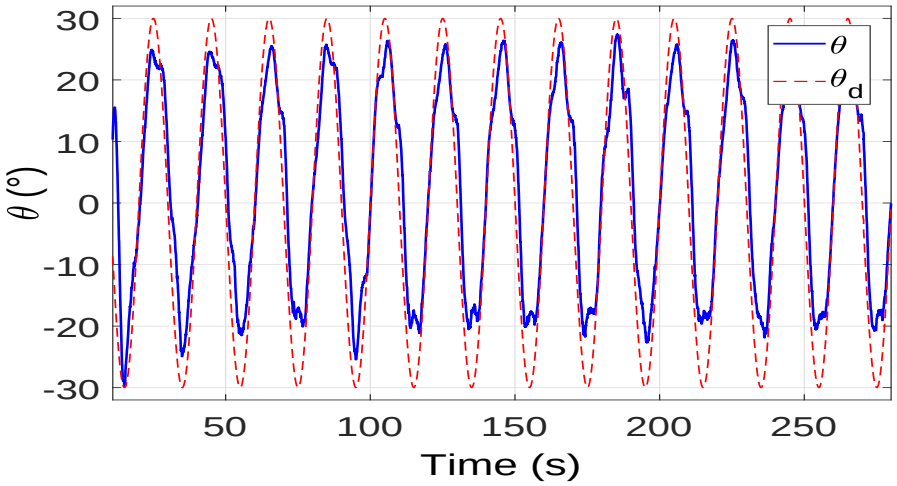

Fig. 22. Pitch performance when appliying a PID controller for following a $\sin(\cdot)$ function with amplitude of $\pm 30°$.

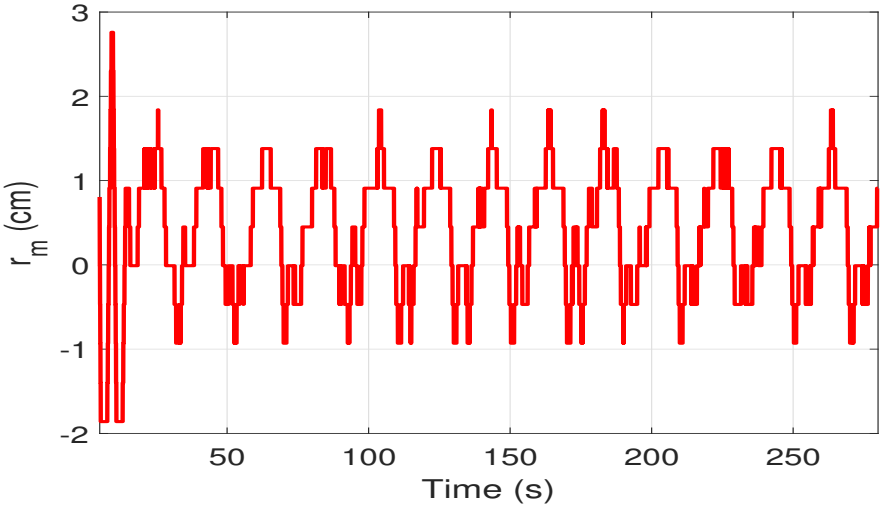

Fig. 23. r_m response when controlling the mobile mass with a PID algorithm.

Observe from Figure 22 that the linear controller follows pretty well the imposed trajectory. Notice also that the controller is not capable to track the trajectory when the nose points towards the bottom ($-30°$), we consider that it is due because a small part of the submarine touches the surface and generates changes in the buoyancy of the vehicle. Remark that in this movement the hydrodynamic effects are stronger and a nonlinear controller could give a better performance. The radio response of the mobile mass is presented in Figure 23, observe here that when the radio is negative the amplitude is minor, this fact is when the part of the vehicle touches the surface and then the added mass parameters become stronger.

7. Conclusions

A novel underwater vehicle configuration was presented in this paper. This configuration has the operating principle of the Sepiida animal. Movements in this vehicle were achieved using a mobile mass and a ballast tank with a fluid. A prototype with its embedded system was developed for validating this configuration. Experimental tests were carried out for validate the torque produced by changing the radio of the mobile mass and analyzing the pitch dynamics. A linear controller was used for testing the well performance of the prototype.

Future work includes to design a nonlinear controller for stabilizing all the states in the vehicle and test them in real-time experiments.

References

1. D. L. Rudnick, R. E. Davis, C. C. Eriksen, D. M. Fratantoni, and M. J. Perry, "Underwater gliders for ocean research," *Marine Technology Society Journal* **38**(2), 73–84 (2004).
2. S. Cobos-Guzman, J. Torres, and R. Lozano, "Design of an underwater robot manipulator for a telerobotic system," *Robotica* **31**(6), 945–953 (2013).
3. J. Yu, W. Jin, Z. Tan, Y. Huang, Y. Luo, and X. Wang, "Development and experiments of the Sea-Wing7000 underwater glider," *Proceedings of the OCEANS-Anchorage, AK, USA* 1–7 (2017).
4. M. Nakamura, W. Koterayama, H. Kajiwara, J. Noda, I. Takahiro, and M. Naoya, " Development of disk type underwater glider for virtual mooring-part 5, Research on Course Control," *Journal of the Japan Society of Naval Architects and Ocean Engineers* **26** (2017).
5. Ö. Yildiz, R. B. Gökalp, and A. E. Yilmaz, "A review on motion control of the underwater vehicles," *International Conference on Electrical and Electronics Engineering, ELECO. Bursa, Turkey* (IEEE) 11–337 (2009).

6. Y. Ma, G. Pan, Q. Huang, and Y. Shi, "Research on fluid dynamic layout of blend wing body underwater glider with Tail," *OCEANS-MTS/IEEE Kobe Techno-Oceans (OTO)* (IEEE) 1–6 (2018).
7. S. B. Williams, P. Newman, J. Rosenblatt, G. Dissanayake, and H. Durrant-Whyte, "Autonomous underwater navigation and control," *Robotica* **19**(5), 481–496 (2001).
8. T. T. J. Presteros, "Verification of a six-degree of freedom simulation model for the REMUS autonomous underwater vehicle," *Ph.D Thesis Massachusetts institute of technology, Cambridge, MA, USA* (2001).
9. L. Yang, J. Cao, J. Cao, B. Yao, Z. Zeng, and L. Lian, "Hydrodynamic and vertical motion analysis of an underwater glider," *OCEANS-Shanghai, China* (IEEE) 1–6 (2016).
10. B. Claus, R. Bachmayer, and L. Cooney, "Analysis and development of a buoyancy-pitch based depth control algorithm for a hybrid underwater glider," *IEEE/OES Autonomous Underwater Vehicles (AUV). Southampton, UK* (IEEE) pp 1–6 (2012).
11. M. G. Joo, "A controller comprising tail wing control of a hybrid autonomous underwater vehicle for use as an underwater glider," *International Journal of Naval Architecture and Ocean Engineering* (Elsevier) **11**(2), 865–874 (2019).
12. S.-S. Fan, C.-J. Yang, S.-L. Peng, K.-H. Li, Y. Xie, and S.-Y. Zhang, "Underwater glider design based on dynamic model analysis and prototype development," *Journal of Zhejiang University SCIENCE C* **14**(8), 583–599 (2013).
13. J. G. Graver, "Underwater gliders: Dynamics, control and design," *Ph.D Thesis, Faculty of Princeton university, Cite-seer* (2005).
14. J. P. O. Muñiz, and T. S. Jimenez, "VBS design and modelling for a coastal underwater glider," *OCEANS MTS/IEEE Charleston, SC, USA* (IEEE) 1–7 (2018).
15. A. Williams, "Design of a low-cost open-source underwater glide," *engrXiv, Web.* (27 April 2018).
16. I. A. Bustos, T. S. Jiménez, L. G. G. Valdovinos, and M. B. Sánchez, "Stable sliding PD control for underwater gliders: Experimental results," *OCEANS MTS/IEEE, Monterey, CA, USA* (IEEE) 1–7 (2016).
17. B. Jin, J. Gao, and W. Yan,"Pseudo control hedging-based adaptive neural network attitude control of underwater gliders," *OCEANS Aberdeen, UK* (IEEE) 1–5 (2017).
18. N. Mahmoudian, "Efficient motion planning and control for underwater gliders," *Ph.D Thesis Faculty of the Virginia Polytechnic Institute and State University, Virginia, USA* (2009).
19. H. Douglasy, "Instituto Oceanogrfico Woods Hole," *online https://www.whoi.edu/main/slocum-glider 2018* (2018-09-18).
20. E. Y. Hong, H. G. Soon, and M. Chitre, "Depth control of an autonomous underwater vehicle, STARFISH," *OCEANS IEEE-Sydney, NSW, Australia* (IEEE) 1–6 (2010).
21. M. H. Khodayari, and S. Balochian, "Modeling and control of autonomous underwater vehicle (AUV) in heading and depth attitude via self-adaptive fuzzy PID controller," *Journal of Marine Science and Technology, Springer* **20**(3), 559–578 (2015).
22. E. Campos, J. Monroy, H. Abundis, A. Chemori, V. Creuze, and J. Torres, "A nonlinear controller based on saturation functions with variable parameters to stabilize an AUV," *International Journal of Naval Architecture and Ocean Engineering* (Elsevier) **11**(1), 211–224 (2019).
23. J. V. N. de Sousa, A. R. L. de Macêdo, W. F. de Amorim Junior, and de A. G. B. de Lima, "Numerical analysis of turbulent fluid flow and drag coefficient for optimizing the AUV hull design," *Open Journal of Fluid Dynamics, Scientific Research Publishing* **4**(3), 263 (2014).
24. B. H. Jun, J. Y. Park, F. Y. Lee, P. M. Lee, C. M Lee, K. Kim, Y. K Lim, and J. H. Oh, "Development of the AUV ISiMIand a free running test in an Ocean Engineering Basin," *Ocean engineering* (Elsevier) **36**(1), 2–14 (2009).
25. J. Melo, and A. Matos, "Survey on advances on terrain based navigation for autonomous underwater vehicles," *Ocean Engineering* (Elsevier) **139**, 250–264 (2017).
26. E. Snam, "Nomenclature for treating the motion of a submerged body through a fluid JR," *New York: Technical and Research Bulletin*, 1–5 (1952).
27. N. E. Leonard, and J. G. Graver, "Model-based feedback control of autonomous underwater gliders," *IEEE Journal of oceanic engineering* **26**(4), 633–645 (2001).
28. P. Yu, T. Wang, H. Zhou, and C. Shen, "Dynamic modeling and three-dimensional motion simulation of a disk type underwater glider," *International Journal of Naval Architecture and Ocean Engineering* **10**(3), 318–328 (2018).
29. Y. Hang Hou, X. Liang, and X. Yang Mu, "AUV hull lines optimization with uncertainty parameters based on six sigma reliability design," *International Journal of Naval Architecture and Ocean Engineering* **10**(4), 499–507 (2018).
30. Y. C. Sun, and C. C. Cheah, "Adaptive control schemes for autonomous underwater vehicle," *Robotica, Cambridge University Press* **27**(1), 119–129 (2009).
31. R. D. Blevins, and R. Plunkett, "Formulas for natural frequency and mode shape," *Journal of Applied Mechanics* **47**, 461 (1980).
32. J. N. Newman, "Marine hydrodynamics," *MIT press, Cambridge* (2018).
33. C. M. Lee, S. C. Park, J. W. Yu, J. E. Choi, and I. Lee, "Effects of diffraction in regular head waves on added resistance and wake using CFD," *International Journal of Naval Architecture and Ocean Engineering* (Elsevier) **11**(2), 736–749 (2019).